

PAPER • OPEN ACCESS

# Effect of heat treatment on the structural parameters and magnetic properties of copper ferrite nanopowders obtained by the sol-gel combustion

To cite this article: V A Zhuravlev *et al* 2016 *IOP Conf. Ser.: Mater. Sci. Eng.* **110** 012084

View the [article online](#) for updates and enhancements.

## Related content

- [Responses of OH \( \$X^2\$ \) and OH \( \$A^{2+}\$ \) to high-energy electrons of dielectric barrier discharge in plasma-assisted burner flame](#)  
Kazunori Zaima and Koichi Sasaki

# Effect of heat treatment on the structural parameters and magnetic properties of copper ferrite nanopowders obtained by the sol-gel combustion<sup>1</sup>

V A Zhuravlev<sup>1</sup>, E P Naiden<sup>1</sup>, R V Minin<sup>2</sup>, V I Itin<sup>2</sup> and M R Ufimtsev<sup>1</sup>

<sup>1</sup>Tomsk State University, Lenina av., 36, Tomsk, 634050 Russia

<sup>2</sup>Tomsk Scientific Center SB RAS, pr. Akademicheskii 10/4, Tomsk, 634021 Russia

E-mail: ptica@mail.tsu.ru

**Abstract.** Phase composition, structure parameters and basic magnetic characteristics obtained by the sol-gel combustion nanopowders of ferrosinell  $\text{CuFe}_2\text{O}_4$  are investigated. A comparison of the properties of synthesized materials: first sample – immediately after the combustion of the gel and second sample – after annealing at 1073 K for 4 hours are performed. Annealing leads to an increase in the concentration of the phase with tetragonal crystal structure. Particle sizes and the value of anisotropy field of this phase also increased.

## 1. Introduction

Nanosized magnetic particles attracted attention of researchers working in different fields of solid state physic in connection with their rich and often unusual range of properties and applications. This fully applies to the copper ferrite  $\text{CuFe}_2\text{O}_4$ . It is known that the samples of this ferrimagnet may exist in modifications with cubic or tetragonal crystal structures. Implementation of these crystal phases depends on the temperature and conditions of synthesis [1, 2].

According to [1 – 3], the cubic crystal structure with a lattice constant  $a \approx 8.42 \text{ \AA}$  exists in some temperature range below the Curie temperature. The first-order structural phase transition (SPT) into the tetragonal crystal phase with a lattice constant  $a = b \approx 5.82 \text{ \AA}$  and  $c \approx 8.69 \text{ \AA}$  takes place with further cooling. The SPT in the copper ferrites was studied experimentally in [2, 3] with the help of high-resolution neutron diffraction technique. The temperature dependences of the initial magnetic permeability and the parameters of ferromagnetic resonance in the vicinity of the SPT were studied in [4]. In papers [2 – 5] the magnetocrystalline anisotropy of copper ferrites was investigated. It is shown that in the tetragonal phase  $\text{CuFe}_2\text{O}_4$  refers to materials with easy magnetization plane (EMP) and with the large value of anisotropy fields [4, 5].

The investigation of the influence of a size effects on the structural and magnetic properties of this ferrite is of interest. The magnetic properties of nanostructured samples of copper ferrosinells synthesized by different methods were investigated in [6 – 8]. The methods used in this works were: mechanochemical reactions [6], co-precipitation [7] and SHS [8]. It is noted that after the transition to a nanostructured state the value of saturation magnetization increases by about 20 % as compared with bulk samples.

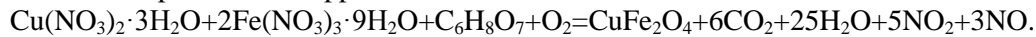
<sup>1</sup> This Research is supported by Tomsk State University Competitiveness Improvement Program reg. N 8.1.23.2015



The results of studies of the properties nanostructured copper ferrite powders obtained by the sol-gel combustion are presented in this paper.

## 2. Preparation of samples

To synthesize the nanoparticles of copper ferrite we used the chemical reaction:



The aqueous solutions with concentration of 1 M: copper nitrate 3-aqueous  $\text{Cu}(\text{NO}_3)_2 \cdot 3\text{H}_2\text{O}$ , iron nitrate 9-aqueous  $\text{Fe}(\text{NO}_3)_3 \cdot 9\text{H}_2\text{O}$ , and citric acid  $\text{C}_6\text{H}_8\text{O}_7$  were pre-prepared. Then they were mixed in accordance with the relationship:

$$\{[\text{Cu}(\text{NO}_3)_2 \cdot 3\text{H}_2\text{O}] : [\text{Fe}(\text{NO}_3)_3 \cdot 9\text{H}_2\text{O}]\} : \text{C}_6\text{H}_8\text{O}_7 = \{1 : 2\} : 2.$$

Concentrated ammonium hydroxide  $\text{NH}_4\text{OH}$  was added dropwise with constant stirring to the obtained solution until  $\text{pH} \approx 2$ . The resultant sol was heated for 3 – 5 hours without boiling. At the evaporation of water it turned into a viscous brown-green gel, which then ignited and burnt. Thus the initial sample No 1 was prepared. The sample No 2 was obtained after the calcinations of initial powder at a temperature of 1073 K for 4 hours.

## 3. The results of x-ray researches

The x-ray analysis was performed using a SHIMADZU XRD-6000 polycrystalline diffractometer. The computer database of x-ray powder diffractometry PDF4+ was used for a qualitative analysis of the phase composition. The quantitative analysis of the phase composition and the refinement of the structural parameters of phases being detected were performed using the program for full profile analysis Powder Cell 2.4.

The results of X-ray diffraction analysis of the samples are summarized in Table 1. According to the table, the product of combustion gel (sample No 1) is a mixture of copper ferrosinels with cubic and tetragonal crystal structure at about equal proportions. This result is quite understandable. The relatively rapid cooling of the reaction product after the combustion process is equivalent to quenching of the gel. The existing at high-temperature non-equilibrium state is retained. Some amount of the hematite phase  $\alpha\text{-Fe}_2\text{O}_3$  is also in sample No 1.

**Table 1.** Phase composition and structural parameters of synthesized materials after combustion sol-gel (sample No 1) and after calcinations (sample No 2).

Sample	Phase composition	Phase content vol. (%)	Parameters of the crystal lattice		Lattice distortion $\gamma_T = c / a\sqrt{2}$	CSR (nm)
			$a$ (Å)	$c$ (Å)		
No 1	$\text{CuFe}_2\text{O}_4$ – tetra.	48	5.830	8.610	1.04	22
	$\text{CuFe}_2\text{O}_4$ – cube.	46	8.335	-	-	80
	$\alpha\text{-Fe}_2\text{O}_3$	6	5.063	13.736	-	15
No 2	$\text{CuFe}_2\text{O}_4$ – tetra.	95	5.826	8.665	1.05	80
	$\text{CuFe}_2\text{O}_4$ – cube.	4	8.416	-	-	16
	$\alpha\text{-Fe}_2\text{O}_3$	1	5.135	13.640	-	15

Calcinations of the sample No 1 followed by slow cooling leads to a significant increase in the content of the tetragonal phase and a significant increase in its coherent scattering region (CSR). The distortion of tetragonal lattice also increased and approached to the thermodynamically equilibrium value that equals to 1.06 [1]. This suggests the diffusion of  $\text{Cu}^{+2}$  ions from tetrahedral to octahedral sublattices during annealing. The obtained values of the lattice constants of the tetragonal and cubic phases are close to the data in [1 – 3].

## 4. Research of the magnetization curves

A study of the magnetization curves in pulsed magnetic fields up to 14 kOe was conducted by the method described in [9]. The values of the specific residual magnetization ( $\sigma_r$ ) and the specific

saturation magnetization ( $\sigma_s$ ) are presented in Table 2. In the last two columns of the table the calculated according to the formula  $M = \sigma \cdot \rho$  values of the magnetizations of unit volume are shown. Here  $\rho = 5.42 \text{ g/cm}^3$  is the X-ray density of ferrimagnets  $\text{CuFe}_2\text{O}_4$  [10].

**Table 2.** The research results of the magnetization curves

Sample	$\sigma_r, \text{Gs} \cdot (\text{cm}^3/\text{g})$	$\sigma_s, \text{Gs} \cdot (\text{cm}^3/\text{g})$	$M_r, \text{Gs}$	$M_s, \text{Gs}$	$M_r/M_s$
No 1	20.6	31.5	112	171	0.66
No 2	22.1	30.9	120	168	0.71

According to Table 2 the saturation magnetization values ( $\sigma_s$ ,  $M_s$ ) of samples No 1 and No 2 are closed. The ratio of  $M_r/M_s$  after annealing increases, which indicates an increase in the coercive force of the material. It should be noted that the value  $M_s$  is more by  $\sim 20\%$  then one given in [1, 10] for a bulk sample magnitude  $M_s \approx 135 \text{ Gs}$ . The same increase in the saturation magnetization of the copper ferrite in the nanostructured state was observed in [6 – 8].

### 5. The study of the magnetic anisotropy by the FMR method

The ferromagnetic resonance (FMR) spectra were measured by the standard waveguide transmission technique in the frequency range 26 – 37 GHz using an automated radio spectroscope. For FMR investigations the powders of samples No 1 and No 2 were charged into quartz tubes with inner diameter of 0.7 mm and length of 10 mm. The density of powder samples was identical and equal to  $\approx 2.6 \text{ g/cm}^3$ .

Investigations of the ferromagnetic resonance spectra of powder and polycrystalline oxide ferrimagnetic materials allowed a number of magnetic parameters of these materials important for practical applications to be determined [11, 12]. Such as: magnitude and sign of magnetocrystalline anisotropy fields ( $H_{ai}$ ); saturation magnetization ( $M_s$ ); value of the gyromagnetic ratio  $\gamma = ge/2mc$ , where  $g$  is the effective  $g$ -factor of the examined material,  $e$  is the electron charge,  $m$  is the electron mass, and  $c$  is the velocity of light.

Figure 1 shows imaginary parts of the diagonal components of the permeability tensor (lines) calculated as described in [12] and measured experimental curves of the FMR (points) samples No 1 (Fig. 1 a) and No 2 (Fig. 1 b). Measurements and calculations were performed for the frequency 36 GHz. The experimental curves are normalized to the theoretical ones. The calculated curves 3 at Figure 1 are total resonance curves, consisting of contributions from the phases with a cubic structure (curve 1) and a tetragonal structure (curves 2).

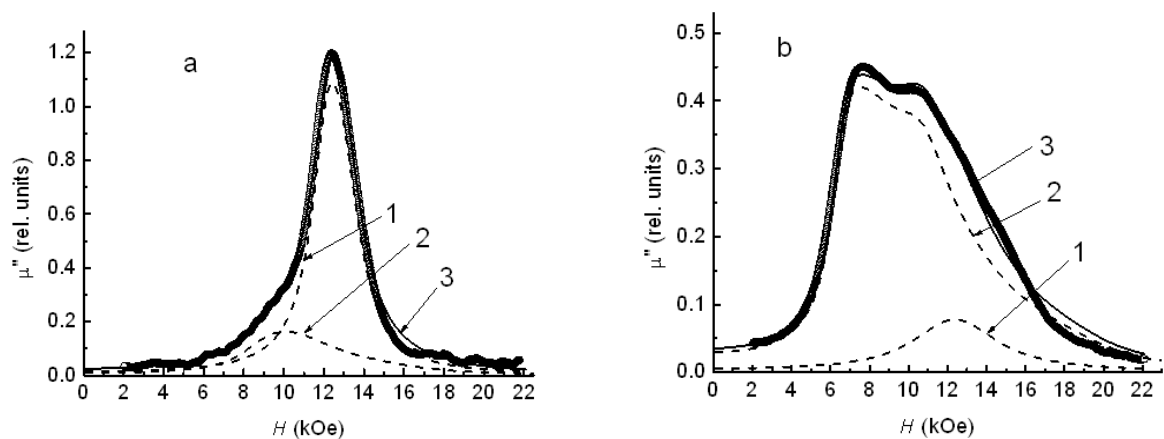


**Figure 1.** The curves of the FMR for sample No 1– a and No 2 – b. Points are the experimental curves. Lines 1 – calculations for the cubic phase, 2 – for the tetragonal phase, 3 – the sum of the curves 1 and 2. Parameters of calculated curves are shown in Table 3.

The shape of experimental FMR curve of sample No 1 corresponds to the materials with low values of the anisotropy fields. The value of the resonant field of this sample is close in magnitude to the resonance field for isotropic material  $H_{\text{res}} = \omega/\gamma = 12.5$  kOe. The rise of the low-field slope of the resonance curve indicates the presence in this material a phase with a large value of anisotropy field. The shape of the experimental resonance curve of the sample No 2 with a predominance of the tetragonal crystal phase is typical for of a materials with magnetic ordering type of EMP (the anisotropy field  $H_0 \leq 0$ ).

The experimental FMR spectra of samples No 1 and No 2 were measured in the frequency range 26 - 37 GHz. The processing of spectra was carried out in two stages. In the first stage, the frequency dependences of the resonance fields were drawn. Then the estimations for magnetomechanical ratios  $\gamma$  and anisotropy fields for cubic ( $H_a$ ) and tetragonal ( $H_0$ ,  $H_{a3}$ ) crystal phases were performed by the least squares method. At the second stage, more accurate values of these parameters and volume concentration of cubic ( $c_k$ ) and tetragonal ( $c_t$ ) phases were determined by a detailed comparison of the shapes of experimental and calculated resonance curves at different frequencies. Note that the values of  $M_s$  for cubic and tetragonal crystal phases are unknown separately. Thus we took their magnetizations  $M_s$  from Table 2 at the calculation of the partial contributions to the total FMR absorption.

Table 3 shows the parameters used to calculate the curves of the FMR samples No 1 and No 2. Here  $c_k$ ,  $c_t$  – are volume concentrations of the phases with cubic and tetragonal structures.  $H_a$ ,  $H_0$ ,  $H_{a3}$  – are the values of anisotropy fields,  $\gamma/2\pi$  – are the magnetomechanical ratios and  $\alpha$  – are decay constants in the Landau-Lifshitz-Gilbert equation for a monocrystalline grain.

**Table 3.** Parameters of the calculated curves

Sample	The phase with low anisotropy (cubic + superparamagnetic tetragonal)				The phase with tetragonal structure				
	$c_k$ (%)	$\gamma/2\pi$ GHz/kOe	$H_a$ , kOe	$\alpha$	$c_t$ (%)	$\gamma/2\pi$ GHz/kOe	$H_0$ , kOe	$H_{a3}$ , kOe	$\alpha$
No 1	75 (48)	2.88	-1.0	0.08	25 (46)	3.10	-5.0	3.0	0.16
No 2	20 (4)	2.88	-1.0	0.15	80 (95)	3.10	-8.0	6.0	0.12

The tabulated for the cubic phase values of the anisotropy fields are rather rough upper estimate. However, they are correlated with the value of  $H_a \approx -890$  Oe obtained from the data of [10] for room temperature. It is interesting to compare our estimation of parameters for the tetragonal crystal phase with the data obtained on the single-crystal sample in [5]. The listed in Table 4 values of  $\gamma/2\pi$  are considerably more than estimation  $\gamma / 2\pi \approx 2.6$  GHz / kOe from [5]. The value of the anisotropy field  $H_0$  of sample No 2 is three times less than  $H_0$  in [5]. As regards the value of the anisotropy field in the basal plane  $H_{a3}$ , it is conversely more then given in [5] at approximately one order of magnitude.

Table 3 shows that the volume concentrations of the phases determined from an experiment on FMR markedly differs from the X-ray diffraction data (Table 1). According to the FMR research of the sample No 1 the concentration of phase with large values of the anisotropy field is almost 25% less than one given from the X-ray diffraction. For the phase with a small quantity of  $H_a$  the situation is reversed. This behavior takes place in the sample №2, wherein the content of phase with low anisotropy field  $H_a$  also increased, and the phases with large anisotropy fields  $H_0$ ,  $H_{a3}$  reduced approximately at 15 % compared with X-ray diffraction data.

Possible reasons for these differences are following. Values of particle sizes on the CSR shown in Table 1 are raw estimations. Part of the particles with small sizes having a tetragonal crystal structure may exist in a superparamagnetic state with a small anisotropy. FMR in such particles occurs at the same values of the magnetic field as in particles with a cubic crystal structure [13].

Smaller values of the anisotropy fields for phase with tetragonal structure of sample No 1 (CSR  $\approx 22$  nm) as compared with the sample No 2 (CSR  $\approx 80$  nm) can also be explained by the influence of

size effects. As noted in the paper [13], with decreasing of a particle sizes the influence of thermal fluctuations on the magnetic properties of the material are increased and the value of the anisotropy field is reduced.

## 6. Conclusion

In the paper the effect of heat treatment on the structural and magnetic properties of copper ferrite nanopowders synthesized by sol-gel combustion is studied. It is shown that the as-prepared powder consists of a mixture of phases with cubic and tetragonal crystal structures with approximately the same concentrations. Annealing leads to a significant increase of content of thermodynamic equilibrium at room temperature tetragonal phase. The value of the saturation magnetization does not change and the anisotropy fields of the tetragonal phase increases significantly. Measured by FMR method parameters of nanostructured copper ferrite differ significantly from the parameters obtained on bulk monocrystalline sample in [5].

## References

- [1] Krupicka S 1976 Physik der Ferrite und der Verwandten Magnetischen Oxide, vol. I *Mir, Moscow* 353 (in Russian).
- [2] Balagurov A M, Bobrikov I A, Pomjakushin V Yu, Sheptyakov D V and Yushankhai V Yu 2015 *J. Magn. Magn. Matter.* **374** 591
- [3] Balagurov A M, Bobrikov I A, Maschenko M S, Sangaa D and Simkin V G 2013 *Crystallography Reports* **58** 710
- [4] Onyszkiewicz I, Malafaev N T, Murakhovskii A A and Pietrzak J 1982 *Phys. Stat. solidi (a)* **73** K243
- [5] Malafaev N T, Murakhovskii A A, Popkov J A and Onyszkiewicz I 1990 *J. Magn. Magn. Matter.* **89** 8
- [6] Jiang J Z, Goya G F and Rechenberg H R 1999 *J. Phys.: Condens. Matter.* **11** 4063
- [7] Pajić D, Zadro K, Vanderberghe R E and Nedkov I 2004 *J. Magn. Magn. Matter.* **281** 353
- [8] Kumar E R, Jayaprakash R, Devi G S and Reddy P S P 2014 *J. Magn. Magn. Matter.* **355** 87
- [9] Kreslin V Yu and Naiden E P 2002 *Prib. Tekh. Eksp.* **1** 63
- [10] Smit J and Wijn H P J 1959 Ferrite. Physical properties of ferrimagnetic oxides in relation to their technical applications. *Philips' Technical Library* 369
- [11] Zhuravlev V A 1999 *Physics of the Solid State* **41** 956
- [12] Zhuravlev V A and Meshcheryakov V A 2014 *Russian Physics Journal* **56** 1387
- [13] Raikher Yu L and Stepanov V I 1994 *Phys. Rev.* **50** 6250